Onset of morphological instability in two binary liquid layers

G. B. McFadden,[1,a)] S. R. Coriell,[1] and P. A. Lott[2]
[1]*National Institute of Standards and Technology, Gaithersburg, Maryland 20899, USA*
[2]*Lawrence Livermore National Lab, Box 808, L-561, Livermore, California 94551, USA*

(Received 28 December 2010; accepted 25 February 2011; published online 11 April 2011)

We consider the linear stability of a horizontal liquid bilayer subject to vertical heating. The two layers consist of a binary liquid that has undergone a phase transition, resulting in a horizontal interphase boundary between two phases with different compositions. We perform linear stability calculations to determine the critical values for the applied temperature difference across the system that is necessary to produce instability using both numerical computations and small-wavenumber approximations. We focus on an instability primarily due to the phase change, which can occur in the absence of buoyancy and surface-tension-driven convection. We find both direct and oscillatory modes of instability, either of which can persist to small wavenumbers that allow approximate analytical descriptions. The interaction of flow with a deforming phase boundary plays a critical role in the instability, and the results are compared to morphological stability results that can be obtained in the absence of flow. [doi:10.1063/1.3567188]

I. INTRODUCTION

The stability of a fluid-fluid interface is important in a number of scientific and technological applications.[1–4] In previous work,[5] we have considered the linear stability of a two-phase binary liquid confined between differentially heated horizontal parallel plates in a layer geometry and subject to the effects of buoyancy and thermocapillarity. The two liquid phases are not considered to be immiscible, but are in thermodynamic equilibrium. An example is a liquid that has undergone phase separation at a temperature below the critical point (the temperature at which the phases become identical). The two phases are separated by a deformable interphase boundary with a temperature-dependent surface energy that can give rise to Marangoni convection in addition to Rayleigh–Benard convection. In the previous paper,[5] we found a mode of instability even in the absence of buoyancy and thermocapillarity, which is therefore a phase-change mode of instability reminiscent of the familiar morphological instability in two-phase systems subject to transport by diffusion and heat flow.[6] This mode was examined for the aluminum-indium system, sufficiently far from the critical point that the usual transport equations are valid with a sharp interface model. The density ratio ρ^* of the two phases at the temperature considered ($\rho_{\mathrm{Al}}/\rho_{\mathrm{In}}=0.427$) differs significantly from unity, so that dynamic perturbations to the interface shape drive fluid motion normal to the interface. However, in many two-phase systems, especially in organic systems, for example, the acetone-hexadecane system,[7] the density ratio can approach unity. For this case, it is conceivable that flow effects could be negligible in determining the stability of the system. In this paper, we consider the linear stability of two binary liquid layers with equal densities in the absence of buoyancy and thermocapillarity, and find unstable phase-change modes, including both direct modes and oscillatory modes that occur over a range of wavenumbers, including small wavenumbers where analytical approximations can be obtained that illustrate directly the effects of flow on the modes. In addition, in this paper we generalize an approximate dispersion relation for small wavenumbers obtained in our previous work that had the form

$$\mathcal{G}=\frac{(\rho^*-1)\mathrm{Bo}}{c_0\ \mathrm{Ma}\ \mathrm{Cr}}, \tag{1}$$

where $\mathcal{G}$ is a dimensionless temperature gradient (defined below), Bo is the Bond number, Ma is the Marangoni number, Cr is the Crispation number, and c_0 is a constant that depends on the depth ratio, the viscosity ratio, and the thermal conductivity ratio. This approximation describes a direct mode of Marangoni-driven instability for small wavenumbers in the absence of buoyancy, giving a finite value for the critical dimensionless temperature gradient $\mathcal{G}$. This approximation breaks down for either equal densities in each phase ($\rho^*=1$) or in the absence of surface tension gradients (Ma $=0$). In this work, we extend this analysis, obtaining a modified dispersion relation that describes in addition the cases $\rho^*=1$ and/or Ma$=0$. For $\rho^*=1$ numerical calculations for the full problem show that the critical value of $\mathcal{G}$ scales with the square of the wavenumber a, and in addition, a small-wavenumber instability is found for Ma$=0$ that is also convectively driven; the scaling of this mode with wavenumber is also sensitive to whether or not the densities are equal. The modified small-number expansion is found to take the form

$$\mathcal{G}=\frac{(\rho^*-1)\mathrm{Bo}-a^2}{c_0\ \mathrm{Ma}\ \mathrm{Cr}+c_1\ \mathrm{Cr}}, \tag{2}$$

where the constant c_1 also depends on the depth ratio and thermophysical properties. The new term proportional to c_1 requires the careful retention of $O(a^2)$ terms that were neglected previously.[5]

[a)]Electronic mail: mcfadden@nist.gov.

The outline of the paper is as follows. In Sec. II we describe the model, including a summary of the thermodynamics and governing equations. Numerical results are given in Sec. III, followed by a summary of some small-wavenumber expansions in Sec. IV. An analysis of a simplified no-flow example is given in Sec. V, and a discussion is provided in Sec. VI.

II. GEOMETRY AND GOVERNING EQUATIONS

We consider a semi-infinite horizontal two-layer system with vertical heating imposed across the layers. The unperturbed system is assumed to be quiescent with a stationary planar interface located at position $z=0$. The unperturbed upper layer (the α phase) extends over the interval $0<z<\bar{H}_\alpha$, and the unperturbed lower layer (the β phase) extends over the interval $-\bar{H}_\beta<z<0$. Without loss of generality, we consider the linear stability results for a two-dimensional system with velocity components u and w in the x and z directions, respectively. The perturbed interface is assumed to have the form $z=h(x,t)$; the horizontal coordinate extends over the interval $-\infty<x<\infty$. The upper boundary at $z=\bar{H}_\alpha$ and the lower boundary at $z=-\bar{H}_\beta$ are assumed to be isothermal and impermeable to solute with no-slip boundary conditions. The equations of motion are given by the Navier–Stokes equations in the Boussinesq approximation,[8] coupled to equations for heat and mass transfer.[9] The interfacial boundary conditions consist of continuity of tangential velocity, conservation of mass, the balance of normal and tangential stress, continuity of temperature, balance of heat and solute fluxes, and the conditions of thermodynamic equilibrium at the interface. The latter conditions express the relationships between interfacial temperature and solute concentrations as depicted in the system's phase diagram. The interfacial conditions for the phase-change system differ from those for an immiscible system primarily because of the possibility of mass transport through the phase boundary, which is not a material interface. Therefore, the two boundary conditions equating the normal velocity of the interface and the normal component of the flow velocity in each phase in an immiscible system are replaced by a single equation for the continuity of the relative mass flux normal to the interface in a phase-change problem. In addition, the conditions of thermodynamic equilibrium that are applied in the phase-change problem augment the usual continuity conditions for temperature and solute that apply in the immiscible case. The generation of latent heat during a phase change also modifies the usual heat flux condition.

A. Base state

We consider a quiescent one-dimensional base state with a static temperature gradient normal to the planar interphase boundary at $z=0$, with interface temperature $T=T_E$ and pressure $p=p_E$, and corresponding equilibrium concentrations $\bar{c}^\alpha$ and $\bar{c}^\beta$. Near these points, the linearized coexistence curve relating temperature and concentration for a fixed pressure $p=p_E$ takes the form

TABLE I. Dimensionless properties used in numerical calculations. Material properties are based on values used for the aluminum-indium system (Ref. 5) with $d=1$ cm, but further idealized by taking $\rho^*=1$, and $\mathrm{Ma}=\mathrm{Ra}=0$.

Mass fraction of indium in the α phase	c^α	0.1721
Mass fraction of indium in the β phase	c^β	0.9650
Density ratio	$\rho^*=\rho^\alpha/\rho^\beta$	1.0
Kinematic viscosity ratio	$\nu^*=\nu^\alpha/\nu^\beta$	3.818
Dynamic viscosity ratio	$\mu^*=\mu^\alpha/\mu^\beta$	1.630
Thermal diffusivity ratio	$\kappa^*=\kappa^\alpha/\kappa^\beta$	1.137
Thermal conductivity ratio	$k^*=k^\alpha/k^\beta$	1.664
Thermal expansion ratio	$\eta^*=\eta^\alpha/\eta^\beta$	1.127
Diffusivity ratio	$D^*=D^\alpha/D^\beta$	1.0
Schmidt number	$\mathrm{Sc}=\nu^\beta/D^\beta$	13.2
Prandtl number	$\mathrm{Pr}=\nu^\beta/\kappa^\beta$	3.99×10^{-3}
Bond number	$\mathrm{Bo}=g\rho^\beta d^2/\gamma$	233.1
Crispation number	$\mathrm{Cr}=\mu^\beta\kappa^\beta/d\gamma$	8.420×10^{-5}
Marangoni number	$\mathrm{Ma}=-\gamma_T T_E d/\mu_\beta\kappa_\beta$	0
Rayleigh number	$\mathrm{Ra}=g\eta_\beta T_E d^3/\nu_\beta\kappa_\beta$	0
Dimensionless latent heat	$\mathcal{L}_{\alpha\beta}=\rho_\beta L_{\alpha\beta}\kappa_\beta/k_\beta T_E$	1.287
Dimensionless dT/dc^α	$\tilde{m}_\alpha$	1.218
Dimensionless $-dT/dc^\beta$	$\tilde{m}_\beta$	5.152

$$T=T_E+m^\alpha(c-\bar{c}^\alpha),\quad T=T_E-m^\beta(c-\bar{c}^\beta), \tag{3}$$

where $m^\alpha>0$ and $m^\beta>0$.

The solute field is assumed to be uniform in each phase, and the thermal field is

$$T^\alpha(z)=T_E+G_\alpha z \tag{4}$$

in the α phase and

$$T^\beta(z)=T_E+G_\beta z \tag{5}$$

in the β phase. The temperature gradients in the base state satisfy

$$0=k_\alpha G_\alpha-k_\beta G_\beta, \tag{6}$$

where k_α and k_β are the thermal conductivities in each phase. The pressure field in the base state is hydrostatic. We assume the transport coefficients are uniform in each phase, and, following the Boussinesq approximation, we assume the density is uniform in all terms in the governing equations except for the gravitational term.

B. Dimensionless parameters

We make the equations dimensionless based on a length scale given by the total depth $d=\bar{H}_\alpha+\bar{H}_\beta$, a time scale based on the thermal time d^2/κ_β, the velocity scale κ_β/d, the temperature scale $G_\beta d$, and the pressure scale $\nu_\beta\kappa_\beta\bar{\rho}_\beta/d^2$. Here, ν_β is the kinematic viscosity, κ_β is the thermal diffusivity, and $\bar{\rho}_\beta=\bar{\rho}(T_E,\bar{c}^\beta)$ is the density in the β phase. These scales introduce a number of dimensionless parameters which are listed in Table I. In addition, we define the dimensionless temperature gradient in the β phase,

$$\mathcal{G} = \frac{G_\beta d}{T_E}, \tag{7}$$

and the geometrical parameter $H_\alpha = \bar{H}_\alpha / d$ representing the dimensionless depth of the α phase; the corresponding depth of the β phase is $H_\beta = 1 - H_\alpha$. We consider the temperature gradient G_β to play the role of an experimental control parameter, and so we have chosen to isolate the dependence on G_β in the dimensionless parameters in the single variable $\mathcal{G}$. The conventional Rayleigh number and Marangoni numbers are then given by

$$\mathcal{G}\ \mathrm{Ra} = \frac{g\eta_\beta G_\beta d^4}{\nu_\beta \kappa_\beta}, \quad \mathcal{G}\ \mathrm{Ma} = -\frac{\gamma_T G_\beta d^2}{\mu_\beta \kappa_\beta}, \tag{8}$$

where the parameters Ra, Ma, and the dimensionless latent heat $\mathcal{L}_{\alpha\beta}$, are independent of the temperature gradient and depend only on the geometry and material parameters. The values of the dimensionless parameters used in the calculations are given in Table I. (We have taken $D^* = 1$ since we know of no measurements of this quantity.) Henceforth, all variables will be dimensionless unless otherwise indicated.

C. Linearized governing equations

We assume a horizontal wavenumber a and a temporal growth rate $\sigma = \sigma_r + i\sigma_i$; for example, the perturbed interface $z = h(x,t)$ then has the specific form

$$z = \tilde{h}\exp(iax)\exp(\sigma_r t + i\sigma_i t), \tag{9}$$

where $\tilde{h}$ is the dimensionless interface amplitude. Neutral stability corresponds to $\sigma_r = 0$. A direct mode of instability has $\sigma_i = 0$ ("exchange of stabilities") whereas the case $\sigma_i \neq 0$ represents an oscillatory mode ("overstability"); for this problem, oscillatory modes come in complex conjugate pairs.

The perturbed quantities (indicated by tildes) satisfy the linearized governing equations

$$ia\tilde{u}^\alpha + \tilde{w}_z^\alpha = 0, \tag{10}$$

$$\mathrm{Pr}^{-1}\ \sigma\tilde{u}^\alpha + ia\tilde{p}^\alpha/\rho^* = \nu^*(\tilde{u}_{zz}^\alpha - a^2\tilde{u}^\alpha), \tag{11}$$

$$\mathrm{Pr}^{-1}\ \sigma\tilde{w}^\alpha + \tilde{p}_z^\alpha/\rho^* = \nu^*(\tilde{w}_{zz}^\alpha - a^2\tilde{w}^\alpha) + \eta^*\mathcal{G}\ \mathrm{Ra}\ \tilde{T}^\alpha, \tag{12}$$

$$\sigma\tilde{T}^\alpha + G^*\tilde{w}^\alpha = \kappa^*(\tilde{T}_{zz}^\alpha - a^2\tilde{T}^\alpha), \tag{13}$$

$$\mathrm{Pr}^{-1}\ \mathrm{Sc}\ \sigma\tilde{c}^\alpha = D^*(\tilde{c}_{zz}^\alpha - a^2\tilde{c}^\alpha) \tag{14}$$

for $z > 0$ and

$$ia\tilde{u}^\beta + \tilde{w}_z^\beta = 0, \tag{15}$$

$$\mathrm{Pr}^{-1}\ \sigma\tilde{u}^\beta + ia\tilde{p}^\beta = \tilde{u}_{zz}^\beta - a^2\tilde{u}^\beta, \tag{16}$$

$$\mathrm{Pr}^{-1}\ \sigma\tilde{w}^\beta + \tilde{p}_z^\beta = \tilde{w}_{zz}^\beta - a^2\tilde{w}^\beta + \mathcal{G}\ \mathrm{Ra}\ \tilde{T}^\beta, \tag{17}$$

$$\sigma\tilde{T}^\beta + \tilde{w}^\beta = \tilde{T}_{zz}^\beta - a^2\tilde{T}^\beta, \tag{18}$$

$$\mathrm{Pr}^{-1}\ \mathrm{Sc}\ \sigma\tilde{c}^\beta = (\tilde{c}_{zz}^\beta - a^2\tilde{c}^\beta) \tag{19}$$

for $z < 0$. Here, $\tilde{w}_z^\alpha$ denotes the partial derivative $\partial\tilde{w}^\alpha/\partial z$, etc.

The boundary conditions at $z = 0$ are continuity of tangential velocity and conservation of mass,

$$\tilde{u}^\alpha - \tilde{u}^\beta = 0, \tag{20}$$

$$\rho^*(\tilde{w}^\alpha - \sigma\tilde{h}) = (\tilde{w}^\beta - \sigma\tilde{h}), \tag{21}$$

balance of normal and tangential stress,

$$(\tilde{p}^\alpha - \tilde{p}^\beta) - \mathrm{Bo}\ \mathrm{Cr}^{-1}(\rho^* - 1)\tilde{h} + a^2\ \mathrm{Cr}^{-1}\ \tilde{h} = 2(\mu^*\tilde{w}_z^\alpha - \tilde{w}_z^\beta), \tag{22}$$

$$(\mu^*\tilde{u}_z^\alpha - \tilde{u}_z^\beta) + ia(\mu^*\tilde{w}^\alpha - \tilde{w}^\beta) - ia\mathcal{G}\ \mathrm{Ma}(\tilde{T}^\alpha + G^*\tilde{h}) = 0, \tag{23}$$

continuity of temperature,

$$\tilde{T}^\alpha + G^*\tilde{h} = \tilde{T}^\beta + \tilde{h}, \tag{24}$$

thermodynamic equilibrium,

$$\mathcal{G}[\tilde{T}^\alpha + G^*\tilde{h}] = \tilde{m}_\alpha\tilde{c}^\alpha, \tag{25}$$

$$\mathcal{G}[\tilde{T}^\alpha + G^*\tilde{h}] = -\tilde{m}_\beta\tilde{c}^\beta, \tag{26}$$

and balance of heat and solute fluxes,

$$\mathcal{G}(k^*\tilde{T}_z^\alpha - \tilde{T}_z^\beta) = \rho^*(\tilde{w}^\alpha - \sigma\tilde{h})\mathcal{L}_{\alpha\beta}, \tag{27}$$

$$D^*\tilde{c}_z^\alpha - \tilde{c}_z^\beta = \mathrm{Pr}^{-1}\ \mathrm{Sc}\ \rho^*(\tilde{w}^\alpha - \sigma\tilde{h})\{\bar{c}^\alpha - \bar{c}^\beta\}. \tag{28}$$

As in our previous work,[5] we have ignored pressure perturbations in Eqs. (25) and (26) since their effects are negligible for the wavenumbers considered here. The effect of capillarity is included directly in the Crispation number in the normal stress balance (22).

III. RESULTS WITH FLOW

We computed the solution numerically using two methods as described previously.[4,5] A matrix collocation procedure, based on a pseudospectral Chebyshev discretization of the solution,[10] provides an approximate set of growth rates for a given wavenumber and value of $\mathcal{G}$. In a complementary shooting procedure, a single growth rate is obtained by using the two-point boundary value solver BVSUP.[11] The resulting modes would take the form of a set of convection rolls on either side of a sinusoidally distorted interface in a two-dimensional geometry.

In Fig. 1 we show a plot of the marginal values ($\sigma_r = 0$) of $\mathcal{G}$ versus wavenumber a for equal layer depths $H_\alpha = H_\beta = 1/2$ with Ra = Ma = 0 and $\rho^* = 1$. For equal depths, the system is stable for positive values of $\mathcal{G}$. At small wavenumbers, the system exhibits a direct mode of instability ($\sigma_i = 0$) indicated by the solid curve; the system is unstable ($\sigma_r > 0$) for sufficiently negative values of $\mathcal{G}$. The marginal values of $\mathcal{G}$ tend to zero for small wavenumbers. An oscillatory mode branches from the direct mode near $a = 2.5 \times 10^{-3}$ as indicated by the dashed curve, so that for larger wavenumbers the system first becomes overstable ($\sigma_i \neq 0$) for sufficiently

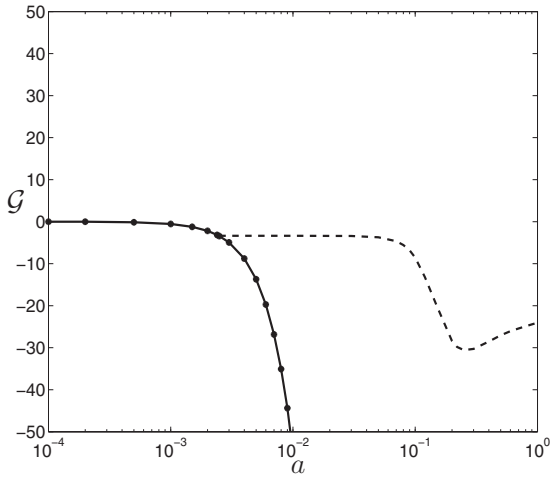

FIG. 1. A plot of $\mathcal{G}$ vs wavenumber a for neutral modes with equal layer depths $H_\alpha = H_\beta = 1/2$ showing morphological instability with flow. The solid curve is a direct mode and the dashed curve is an oscillatory mode. A small-wavenumber approximation is indicated by dots.

negative values of $\mathcal{G}$. The frequency σ_i tends to zero where the oscillatory mode merges with the direct mode, and increases monotonically with increasing wavenumber, reaching $\sigma_i = \pm 3.25$ for $a=1$. The frequency of the oscillatory mode is sensitive to capillarity: for example, decreasing the Crispation number by an order of magnitude increases σ_i to ± 10.22 for $a=1$, while $\mathcal{G}$ is only slightly changed. The behavior of the direct mode at small wavenumbers can be described analytically by a small-wavenumber approximation which we present below; these results are indicated by dots in the figure.

In Fig. 2 we show a plot of $\mathcal{G}$ versus wavenumber a for $H_\alpha = 0.1$ and $H_\beta = 0.9$. There is again a direct mode of instability at small wavenumbers (solid curve), but now the instability occurs for sufficiently large positive values of $\mathcal{G}$. An

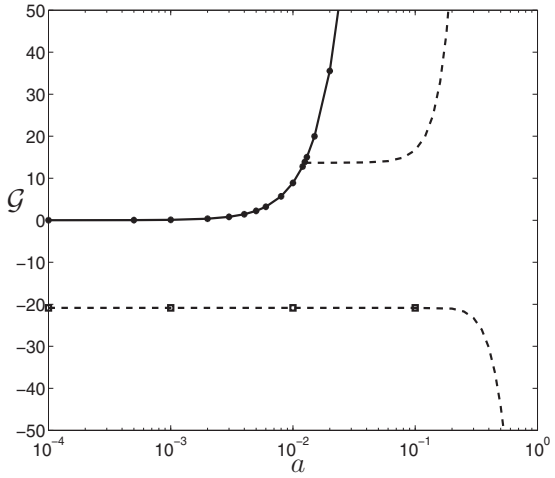

FIG. 2. A plot of $\mathcal{G}$ vs wavenumber a for neutral modes with layer depths $H_\alpha = 0.1$ and $H_\beta = 0.9$ showing morphological instability with flow. The solid curve is a direct mode and the dashed curves are oscillatory modes. The round data points indicate the results from a small-wavenumber approximation for the direct mode, and the square data points on the oscillatory branch correspond to analytical results for a morphological stability analysis in which flow is neglected.

oscillatory mode (dashed curve) branches from the direct mode at $a = 1.25 \times 10^{-2}$, and the marginal values of $\mathcal{G}$ rise rapidly with increasing wavenumber while the values of σ_i remain relatively small with $\sigma_i = \pm 1.0 \times 10^{-3}$ for $a=0.25$. The system is linearly stable for small negative values of $\mathcal{G}$, but becomes unstable to another oscillatory mode when $\mathcal{G}$ becomes sufficiently negative. This oscillatory mode asymptotes to a constant value of $\mathcal{G} = -21$ and $\sigma_i = \pm 0.02$ for small wavenumbers. This mode can be described by a simplified dispersion relation in which flow is neglected, as we describe in the Appendix. The corresponding results are shown as the square data points in Fig. 2. The numerical results indicate that for large enough wavenumbers the system becomes stable for finite values of $\mathcal{G}$ of either sign. The small-wavenumber approximation, shown as the dots on the direct mode, reproduces the observed sign change of the critical values of $\mathcal{G}$ as the relative depths of the layers change in passing from Fig. 1 to Fig. 2.

The accuracy of the numerical calculations is found to deteriorate significantly for very small wavenumbers ($a < 10^{-4}$), but we have performed a small-wavenumber expansion for the direct mode that extends the numerical results to this regime, as we describe next.

IV. SMALL-WAVENUMBER APPROXIMATION WITH FLOW

An approximate description of the direct mode of instability with $\mathrm{Ra} = \mathrm{Ma} = 0$ and $\rho^* = 1$ can be obtained in the limit of small wavenumbers; this mode is sensitive to the interface deformation and requires a nonzero value of Cr. A formal expansion can be obtained in terms of a small parameter ϵ representing the ratio of vertical to horizontal length scales in the spirit of a lubrication approximation.[1] By directly examining the dominant terms in the governing equations based on their numerical solution, we find appropriate scalings for the dependent variables with ϵ. If we scale the interface deformation to order unity and scale the wavenumber according to $a = \epsilon \hat{a}$ (denoting scaled variables with a hat), the additional scalings are found to take the form $\tilde{u}^j(z) = \epsilon^3 \hat{u}^j(z)$, $\tilde{w}^j(z) = \epsilon^4 \hat{w}^j(z)$, $\tilde{p}^j(z) = \epsilon^2 \hat{p}^j(z)$, $\tilde{T}^j(z) = \hat{T}^j(z)$, $\tilde{c}^j(z) = \epsilon^2 \hat{c}_0^j(z) + \epsilon^4 \hat{c}_1^j(z)$, and $\mathcal{G} = \epsilon^2 \hat{\mathcal{G}}$, for $j = \alpha$ or β, with all other parameters taken to be of order unity. Note that two terms are necessary to approximate the solute field; the leading order term turns out to be uniform, $\hat{c}_0^j = \text{const}$, but a higher order correction is needed that provides a nontrivial solute flux at the interface to balance the convective contribution. Consistent with these scalings, we find that a simplified set of approximate equations and the boundary conditions are (in terms of the original unscaled variables)

$$ia\tilde{u}^\alpha + \tilde{w}_z^\alpha = 0, \tag{29}$$

$$ia\tilde{p}^\alpha = \mu^* \tilde{u}_{zz}^\alpha, \tag{30}$$

$$\tilde{p}_z^\alpha = 0, \tag{31}$$

$$\tilde{T}_{zz}^\alpha = 0, \tag{32}$$

$$\tilde{c}^{\alpha}_{zz} - a^2\tilde{c}^{\alpha} = 0 \tag{33}$$

for $z>0$ and

$$ia\tilde{u}^{\beta} + \tilde{w}^{\beta}_{z} = 0, \tag{34}$$

$$ia\tilde{p}^{\beta} = \tilde{u}^{\beta}_{zz}, \tag{35}$$

$$\tilde{p}^{\beta}_{z} = 0, \tag{36}$$

$$\tilde{T}^{\beta}_{zz} = 0, \tag{37}$$

$$\tilde{c}^{\beta}_{zz} - a^2\tilde{c}^{\beta} = 0 \tag{38}$$

for $z<0$. The approximate boundary conditions at $z=0$ are

$$\tilde{u}^{\alpha} - \tilde{u}^{\beta} = 0, \tag{39}$$

$$\rho^*\tilde{w}^{\alpha} = \tilde{w}^{\beta}, \tag{40}$$

$$(\tilde{p}^{\alpha} - \tilde{p}^{\beta}) - \mathrm{Bo}\ \ \mathrm{Cr}^{-1}(\rho^* - 1)\tilde{h} + a^2\ \ \mathrm{Cr}^{-1}\ \ \tilde{h} = 0, \tag{41}$$

$$(\mu^*\tilde{u}^{\alpha}_{z} - \tilde{u}^{\beta}_{z}) = ia\mathcal{G}\ \ \mathrm{Ma}(\tilde{T}^{\alpha} + G^*\tilde{h}), \tag{42}$$

$$\tilde{T}^{\alpha} + G^*\tilde{h} = \tilde{T}^{\beta} + \tilde{h}, \tag{43}$$

$$\mathcal{G}[\tilde{T}^{\alpha} + G^*\tilde{h}] = \tilde{m}_{\alpha}\tilde{c}^{\alpha}, \tag{44}$$

$$\mathcal{G}[\tilde{T}^{\alpha} + G^*\tilde{h}] = -\tilde{m}_{\beta}\tilde{c}^{\beta}, \tag{45}$$

$$\mathcal{G}(k^*\tilde{T}^{\alpha}_{z} - \tilde{T}^{\beta}_{z}) = 0, \tag{46}$$

$$D^*\tilde{c}^{\alpha}_{z} - \tilde{c}^{\beta}_{z} = \mathrm{Pr}^{-1}\ \ \mathrm{Sc}\ \ \rho^*\tilde{w}^{\alpha}\{\bar{c}^{\alpha} - \bar{c}^{\beta}\}. \tag{47}$$

By including the terms proportional to $\mathrm{Bo}(\rho^*-1)$ in Eq. (41) and Ma in Eq. (42), we are able to include the small-wavenumber expansion results that were obtained previously.[5]

The solutions to the differential equations and the boundary conditions at $z=H_{\alpha}$ and $z=-H_{\beta}$ are given by $\tilde{p}^{\alpha}$ =const, $\tilde{p}^{\beta}$=const,

$$\tilde{u}^{\alpha} = \frac{ia\tilde{p}^{\alpha}}{2\mu^*}(z-H_{\alpha})^2 + E^{\alpha}(z-H_{\alpha}), \tag{48}$$

$$\tilde{u}^{\beta} = \frac{ia\tilde{p}^{\beta}}{2}(z+H_{\beta})^2 + E^{\beta}(z+H_{\beta}), \tag{49}$$

$$\tilde{w}^{\alpha} = \frac{a^2\tilde{p}^{\alpha}}{6\mu^*}(z-H_{\alpha})^3 - \frac{iaE^{\alpha}}{2}(z-H_{\alpha})^2, \tag{50}$$

$$\tilde{w}^{\beta} = \frac{a^2\tilde{p}^{\beta}}{6}(z+H_{\beta})^3 - \frac{iaE^{\beta}}{2}(z+H_{\beta})^2, \tag{51}$$

$$\tilde{T}^{\alpha} = A^{\alpha}(z-H_{\alpha}), \quad \tilde{T}^{\beta} = A^{\beta}(z+H_{\beta}), \tag{52}$$

$$\tilde{c}^{\alpha} = F^{\alpha}\cosh a(z-H_{\alpha}) \approx F^{\alpha}\left[1 + \frac{a^2}{2}(z-H_{\alpha})^2\right], \tag{53}$$

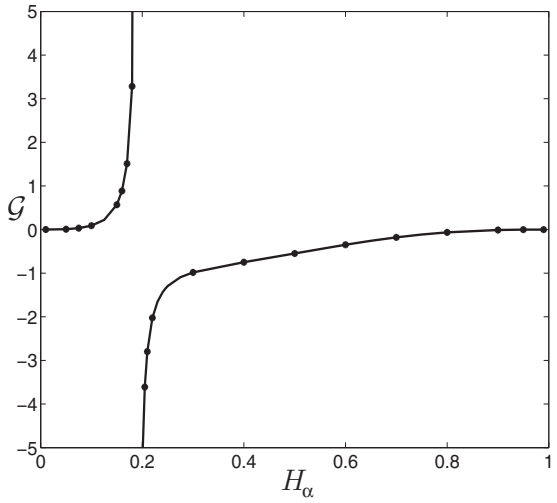

FIG. 3. A plot of $\mathcal{G}$ vs layer depth H_{α} for $\rho^*=1$ and Ma=0 and a wavenumber $a=1.0\times10^{-3}$. The solid curves are the small-wavenumber approximation and the data points are the full numerical solution. There is a pole for $H_{\alpha}=1/(1+D^*\tilde{m}_{\beta}/\tilde{m}_{\alpha})=0.1912$.

$$\tilde{c}^{\beta} = F^{\beta}\cosh a(z+H_{\beta}) \approx F^{\beta}\left[1 + \frac{a^2}{2}(z+H_{\beta})^2\right], \tag{54}$$

where the remaining unknown coefficients are determined by the interfacial boundary conditions at $z=0$. The resulting dispersion relation takes the form

$$\mathcal{G} = \frac{2H_{\alpha}H_{\beta}(H_{\alpha}+\mu^*H_{\beta})(H_{\alpha}+k^*H_{\beta})[\mathrm{Bo}(\rho^*-1)-a^2]}{3(H^2_{\alpha}-\mu^*H^2_{\beta})\mathrm{Ma}\ \ \mathrm{Cr} + c_1\ \ \mathrm{Cr}}, \tag{55}$$

where

$$c_1 = \frac{-36\mu^*(H_{\alpha}+k^*H_{\beta})(\rho^*H_{\alpha}+H_{\beta})(d_1+d_2)\bar{\Lambda}}{H_{\alpha}H_{\beta}}, \tag{56}$$

$$\bar{\Lambda} = \frac{-(D^*H_{\alpha}/\tilde{m}_{\alpha} - H_{\beta}/\tilde{m}_{\beta})}{\mathrm{Pr}^{-1}\ \ \mathrm{Sc}\ \ \rho^*\{\bar{c}^{\alpha}-\bar{c}^{\beta}\}[H_{\alpha}+k^*H_{\beta}]}, \tag{57}$$

$$d_1 = \frac{-\mu^*H_{\alpha}H_{\beta}(4\rho^*H_{\alpha}+3H_{\beta}) - \rho^*H^3_{\alpha}}{6\mu^*H_{\beta}(\rho^*H_{\alpha}+H_{\beta})}, \tag{58}$$

$$d_2 = \frac{-\mu^*H^3_{\beta} - H_{\alpha}H_{\beta}(3\rho^*H_{\alpha}+4H_{\beta})}{6H_{\alpha}(\rho^*H_{\alpha}+H_{\beta})}. \tag{59}$$

For $c_1=0$ and $a^2=0$, this result reproduces the expression for $\mathcal{G}$ given in Eq. (4.6) of Ref. 5. Since $(d_1+d_2)<0$, for Ma =0 and $\rho^*=1$ the sign of $\mathcal{G}$ is determined by that of $\bar{\Lambda}$, which in turn is determined by the sign of $(D^*H_{\alpha}/\tilde{m}_{\alpha} - H_{\beta}/\tilde{m}_{\beta})/(\bar{c}^{\alpha}-\bar{c}^{\beta})$. For fixed material properties, there is a sign change when the ratio of layer depths is varied with a pole of $\mathcal{G}$ for $H_{\alpha}=1/(1+D^*\tilde{m}_{\beta}/\tilde{m}_{\alpha})$ (see Fig. 3). Near this pole, there is enhanced stability as the magnitude of the critical temperature gradient required for instability becomes large.

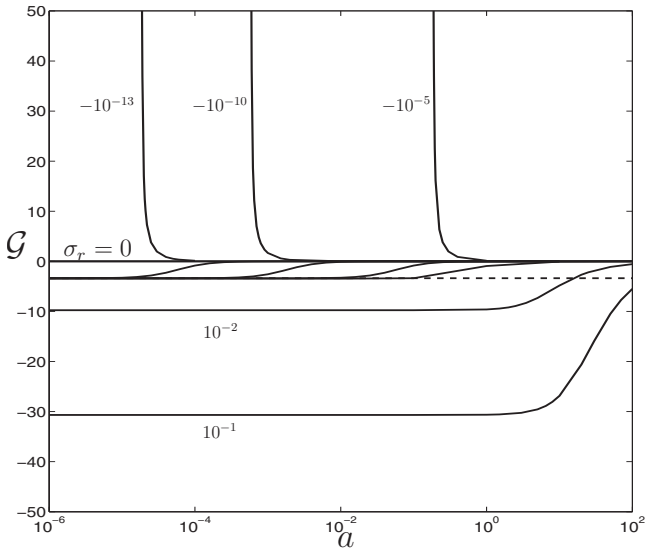

FIG. 4. A plot of $\mathcal{G}$ vs wavenumber a for $H_\alpha = H_\beta = 1/2$ and various values of σ_r showing morphological stability without flow. The dashed line is $\mathcal{G}_0$, the small-wavenumber expansion result for small positive values of σ_r. The numbers in the figure denote the value of σ_r used to generate the adjacent curve. The four additional curves that lie in the narrow region $\mathcal{G}_0 < \mathcal{G} < 0$ correspond to values $\sigma_r = 10^{-12}$, 10^{-9}, 10^{-6}, and 10^{-4} from left to right.

V. RESULTS WITHOUT FLOW

The simplest conventional morphological stability analysis (cf., e.g., Refs. 6 and 12) for a solid-liquid binary system neglects flow in the liquid phase, and the transport equations are purely diffusive in nature. For the fluid-fluid system we consider here, if flow is neglected the normal component of the interfacial momentum balance reduces to

$$(\tilde{p}^\alpha - \tilde{p}^\beta) - \mathrm{Bo}\ \mathrm{Cr}^{-1}(\rho^* - 1)\tilde{h} + a^2\ \mathrm{Cr}^{-1}\ \tilde{h} = 0. \tag{60}$$

Thus, either capillarity ($\mathrm{Cr}^{-1} \neq 0$) or a density difference ($\mathrm{Bo}[\rho^* - 1] \neq 0$) causes a pressure difference across a nonplanar interface ($\tilde{h} \neq 0$). On the other hand, the horizontal momentum equation requires the pressure to vanish if there is no flow, so the equations without flow are not consistent in this case. (In the case of the solid-liquid system, the pressure is often assumed to vanish in the liquid phase, and any pressure is implicitly accounted for in the solid phase, which is assumed to be capable of withstanding arbitrary forces.) Nevertheless, it is useful to perform a linear stability analysis without flow for comparison purposes, which we examine in the Appendix. To do so, we assume the densities are equal, eliminating density-driven convection, and neglect the effects of capillarity ($\mathrm{Cr}^{-1} = 0$). In this case, the momentum conservation equations in the bulk and at the interface are also identically satisfied, and a purely diffusive model can be solved.

Numerical results for the case of equal depths $H_\alpha = H_\beta = 0.5$ are shown in Fig. 4. The system is stable for positive values of $\mathcal{G}$, and unstable for negative values, and has a neutral mode ($\sigma = 0$) for $\mathcal{G} = 0$. Curves for other values of σ_r (with $\sigma_i = 0$) are also shown in Fig. 4. For small positive values of σ_r, the small-wavenumber behavior represents a nonuniform (singular) limit, in that

$$\mathcal{G}_0 = \lim_{\sigma_r \to 0^+} [\lim_{a \to 0^+} \mathcal{G}] \neq \lim_{a \to 0^+} [\lim_{\sigma_r \to 0^+} \mathcal{G}] = 0, \tag{61}$$

where

$$\mathcal{G}_0 = \frac{(k^* H_\beta + H_\alpha) m_\alpha m_\beta (\bar{c}_\alpha - \bar{c}_\beta)}{m_\beta H_\alpha - m_\alpha H_\beta}. \tag{62}$$

This result is shown as the dashed line in Fig. 4, corresponding to $\mathcal{G}_0 = -3.37$. The four curves in Fig. 4 corresponding to $\sigma_r = 10^{-12}$, 10^{-9}, 10^{-6}, and 10^{-4} illustrate this nonuniform behavior.

A large wavenumber expansion of the dispersion relation (A16) in the Appendix gives a direct mode of instability with the leading order behavior

$$\mathcal{G} \sim \frac{\sigma_r}{2a}\left[-\mathcal{L}_{\alpha\beta} + (1 + k^*)\frac{\mathrm{Pr}}{\mathrm{Sc}}\frac{m_\alpha m_\beta (\bar{c}_\alpha - \bar{c}_\beta)}{(D^* m_\beta - m_\alpha)} \right], \tag{63}$$

which is negative for $\sigma_r > 0$ with our parameter values. For the case $H_\alpha = 0.1$ and $H_\beta = 0.9$, the dispersion relation without flow given in Eq. (A16) gives oscillatory modes ($\sigma_i \neq 0$), as shown in Fig. 2.

VI. DISCUSSION

We have performed linear stability calculations for horizontal liquid bilayers in a two-component system that can undergo a phase transformation. Aside from the interphase boundary that is initially present, we assume no further phase transformations occur in the bulk layers, such as nucleation or spinodal decomposition. We have obtained values for the applied temperature difference across the system that is necessary to produce instability by a linear stability analysis using numerical and small-wavenumber approximations. We find a direct phase-change instability due to the combined effects of solute diffusion and fluid flow that persist at small wavenumbers. We find oscillatory instabilities at finite wavenumbers in which flow plays an important role, and in some instances (cf. Fig. 2) we also find an oscillatory instability, where flow is relatively unimportant, which persists at small wavenumbers. This oscillatory mode has a relatively large value of $|\mathcal{G}|$ on the order of 20; since the applied temperature difference across the system is $\delta T \approx \mathcal{G} T_E$, this requires substantial temperature variations for typical values of T_E (e.g., 10^3 K). On the other hand, the direct mode has a small-wavenumber instability with $\mathcal{G}$ tending to zero, so that instability can occur for small values of δT at the cut-off wavenumber set by the lateral length scale of a typical container.

For the two-layer system with phase change, the direct mode persists to small wavenumbers with a scaling that depends on the Crispation and Bond numbers [see Eq. (55)]. In particular, if Cr and Bo are considered to be independent parameters, then for nonzero values of $(\rho^* - 1)\mathrm{Bo}$ and Cr the direct mode has a finite limiting value of the critical temperature gradient $\mathcal{G}$ as the wavenumber tends to zero, whereas if $(\rho^* - 1)\mathrm{Bo} = 0$, $\mathcal{G}$ tends to zero as a^2. Similar behavior is observed for the case of inert fluids for the direct Marangoni instability ($\mathrm{Ma} \neq 0$), see Ref. 1, although we emphasize that the phase-change mode considered in the present paper occurs for $\mathrm{Ma} = 0$. In addition, for the inert Marangoni mode

there is a small-wavenumber instability even with a nondeforming interface (Cr=0) with $\mathcal{G}$ scaling with $1/a^2$, see Refs. 1 and 13; in this case, the mode is insensitive to the Bond number. Similarly, in the single-component liquid-vapor problem considered in Ref. 4, the direct mode of instability with Ma=0 occurs even with a rigid interface (Cr=0). In that case, the small-wavenumber instability is driven by a coupling between interfacial temperature and pressure through the Clausius–Clapeyron effect.[4] By contrast, in the binary case considered here the instability is solute-driven and is accompanied by an interface deformation requiring $\mathrm{Cr}\neq 0$.

In the absence of flow, the morphological stability of a stationary planar interface is usually determined by the presence or absence of undercooled phases. In an applied temperature gradient, one of the phases is heated above the equilibrium temperature, and the other is below (supercooling); for a static interface this results in the marginal state being given by $\mathcal{G}=0$. Constitutional supercooling (effects of solute on the equilibrium temperature) is not an issue for uniform concentrations in the base state. For large wavenumber perturbations, the effects of the confining boundaries become unimportant and the stability analysis is straightforward. For small wavenumbers the effects of the boundaries are significant and the analysis is more complicated; a transcendental dispersion relation is obtained, and the stability results show singularities at certain depth ratios where resonance occurs.

In general, flow effects cannot be neglected even for Ra=Ma=0 and $\rho^*=1$, so the morphological stability results cannot always be expected to provide a useful approximation. The effects of flow on the direct mode of instability at $\mathcal{G}=0$ predicted by the morphological instability analysis shift the instability to nonzero values of $\mathcal{G}$, as shown in Figs. 1 and 2. The direction of the shift is consistent with a stabilization of the mode to higher supercooling required for instability: the direct mode of instability occurs for positive temperature gradients if H_β is near unity (the sample consists mostly of β phase) and occurs for negative temperature gradients if H_α is near unity (the sample consists mainly of α phase), see Fig. 3. This is consistent with a supercooling argument,[12,14] since the liquid in the β phase is supercooled ($T<T_E$) for $\mathcal{G}>0$, and the liquid in the α phase is supercooled for $\mathcal{G}<0$. The oscillatory modes of instability are more difficult to interpret; in particular, we note that for some depth ratios oscillatory instabilities occur for either heating from above or below (see Fig. 2).

For small wavenumbers the effect of the solute field is apparent in the approximate stability relation for the marginal temperature gradient $\mathcal{G}$ given by Eq. (55). For $\rho^*=1$ and Ma=0, $\mathcal{G}$ is inversely proportional to $\bar{\Lambda}$ which depends on the Schmidt number Sc, the liquidus slopes $\tilde{m}_\alpha$ and $\tilde{m}_\beta$, and the solute concentrations $\bar{c}^\alpha$ and $\bar{c}^\beta$. For certain parameter values $\bar{\Lambda}$ can vanish, leading to a pole in $\mathcal{G}$ and hence a strong sensitivity to the solute parameters. Solute dependence is also evident in the large wavenumber approximation given in Eq. (63). We note that these results are obtained for uniform concentrations of solute in the base state. Solute gradients could arise from a nonzero Soret coefficient, which we have neglected in the present work; for the alloy system considered here we are not aware of measurements of the Soret coefficient. Inclusion of the Soret effect could lead to interesting modifications of our stability results.

ACKNOWLEDGMENTS

This work was supported in part by a National Research Council Postdoctoral Fellowship and performed in part under the auspices of the U.S. Department of Energy by Lawrence Livermore National Laboratory under Contract No. DE-AC52-07NA27344.

APPENDIX: STABILITY WITHOUT FLOW

We consider the linear stability problem in the absence of flow effects. The linearized equations are

$$\sigma\tilde{T}^\alpha=\kappa^*(\tilde{T}^\alpha_{zz}-a^2\tilde{T}^\alpha), \tag{A1}$$

$$\mathrm{Pr}^{-1}\ \mathrm{Sc}\ \ \sigma\tilde{c}^\alpha=D^*(\tilde{c}^\alpha_{zz}-a^2\tilde{c}^\alpha) \tag{A2}$$

for $z>0$ and

$$\sigma\tilde{T}^\beta=\tilde{T}^\beta_{zz}-a^2\tilde{T}^\beta, \tag{A3}$$

$$\mathrm{Pr}^{-1}\ \mathrm{Sc}\ \ \sigma\tilde{c}^\beta=\tilde{c}^\beta_{zz}-a^2\tilde{c}^\beta \tag{A4}$$

for $z<0$.

The boundary conditions at $z=0$ are

$$\tilde{T}^\alpha+G^*\tilde{h}=\tilde{T}^\beta+\tilde{h}, \tag{A5}$$

$$\mathcal{G}[\tilde{T}^\alpha+G^*\tilde{h}]=\tilde{m}_\alpha\tilde{c}^\alpha, \tag{A6}$$

$$\mathcal{G}[\tilde{T}^\alpha+G^*\tilde{h}]=-\tilde{m}_\beta\tilde{c}^\beta, \tag{A7}$$

$$\mathcal{G}(k^*\tilde{T}^\alpha_z-\tilde{T}^\beta_z)=-\sigma\mathcal{L}_{\alpha\beta}\tilde{h}, \tag{A8}$$

$$D^*\tilde{c}^\alpha_z-\tilde{c}^\beta_z=-\sigma\ \mathrm{Pr}^{-1}\ \mathrm{Sc}\{\bar{c}^\alpha-\bar{c}^\beta\}\tilde{h}. \tag{A9}$$

We define $\Lambda_\alpha=\sqrt{a^2+\sigma/\kappa^*}$, $\Lambda_\beta=\sqrt{a^2+\sigma}$, $\Omega_\alpha=\sqrt{a^2+\mathrm{Sc}\ \sigma/(\mathrm{Pr}\ D^*)}$, and $\Omega_\beta=\sqrt{a^2+\mathrm{Sc}\ \sigma/\mathrm{Pr}}$. The solutions are

$$\tilde{T}^\alpha=A^\alpha\sinh\Lambda_\alpha(z-H_\alpha),\quad \tilde{T}^\beta=A^\beta\sinh\Lambda_\beta(z+H_\beta), \tag{A10}$$

$$\tilde{c}^\alpha=B^\alpha\cosh\Omega_\alpha(z-H_\alpha),\quad \tilde{c}^\beta=B^\beta\cosh\Omega_\beta(z+H_\beta). \tag{A11}$$

Define

$$\Delta=k^*\Lambda_\alpha\cosh\Lambda_\alpha H_\alpha\sinh\Lambda_\beta H_\beta+\Lambda_\beta\sinh\Lambda_\alpha H_\alpha\cosh\Lambda_\beta H_\beta. \tag{A12}$$

The temperature equations then give

$$A^\alpha=\left[\frac{(G^*-1)\mathcal{G}\Lambda_\beta\cosh\Lambda_\beta H_\beta-\sigma\mathcal{L}_{\alpha\beta}\sinh\Lambda_\beta H_\beta}{\mathcal{G}\Delta}\right]\tilde{h}. \tag{A13}$$

Then,

$$B^{\alpha} = \frac{\mathcal{G}G^{*}\Delta - \sinh \Lambda_{\alpha}H_{\alpha}(G^{*}-1)\mathcal{G}\Lambda_{\beta}\cosh \Lambda_{\beta}H_{\beta} + \sigma\mathcal{L}_{\alpha\beta}\sinh \Lambda_{\alpha}H_{\alpha}\sinh \Lambda_{\beta}H_{\beta}}{\Delta\tilde{m}_{\alpha}\cosh \Omega_{\alpha}H_{\alpha}}\tilde{h}, \tag{A14}$$

$$B^{\beta} = \frac{-\mathcal{G}G^{*}\Delta + \sinh \Lambda_{\alpha}H_{\alpha}(G^{*}-1)\mathcal{G}\Lambda_{\beta}\cosh \Lambda_{\beta}H_{\beta} - \sigma\mathcal{L}_{\alpha\beta}\sinh \Lambda_{\alpha}H_{\alpha}\sinh \Lambda_{\beta}H_{\beta}}{\Delta\tilde{m}_{\beta}\cosh \Omega_{\beta}H_{\beta}}\tilde{h}. \tag{A15}$$

The dispersion relation is then

$$\begin{aligned}\mathcal{G}\{&\Lambda_{\beta}\sinh \Lambda_{\alpha}H_{\alpha}\cosh \Lambda_{\beta}H_{\beta} \\ &+ \Lambda_{\alpha}\cosh \Lambda_{\alpha}H_{\alpha}\sinh \Lambda_{\beta}H_{\beta}\} \\ &= \frac{\Delta\ \mathrm{Pr}^{-1}\ \mathrm{Sc}\ m_{\alpha}m_{\beta}(\bar{c}_{\alpha}-\bar{c}_{\beta})\sigma}{D^{*}m_{\beta}\Omega_{\alpha}\tanh \Omega_{\alpha}H_{\alpha} - m_{\alpha}\Omega_{\beta}\tanh \Omega_{\beta}H_{\beta}} \\ &- \sigma\mathcal{L}_{\alpha\beta}\sinh \Lambda_{\alpha}H_{\alpha}\sinh \Lambda_{\beta}H_{\beta}.\end{aligned} \tag{A16}$$

We note that for a direct mode with $\sigma_i=0$, this relation immediately gives $\mathcal{G}$ as a function of a and σ_r; in particular, $\mathcal{G}=0$ for $\sigma=0$. More generally, we obtain a transcendental equation for σ as a function of a and $\mathcal{G}$, which we solve numerically[15] to determine the oscillatory modes. It is difficult to obtain analytical small-wavenumber approximations to these modes because the quantity $\mathrm{Sc}\ \sigma_i/\mathrm{Pr}$ that appears in Ω_{α} and Ω_{β} is of order unity, so that the dispersion relation remains transcendental in this limit. The solution is further complicated by the possibility of poles where the denominator vanishes, which can occur for certain depth ratios, and other poles associated with vanishing values of the arguments of Λ_{α}, Λ_{β}, Ω_{α}, and Ω_{β}, which can occur for finite wavenumbers if $\sigma_r<0$. The values of $\mathcal{G}$ that occur near these poles are unphysically large and lie outside the range of validity of the Boussinesq approximation; it is also likely that the linearized equations break down near these resonances, requiring a nonlinear theory to obtain consistent results.

[1] S. H. Davis, "Thermocapillary instabilities," Annu. Rev. Fluid Mech. **19**, 403 (1987).
[2] D. D. Joseph and Y. Y. Renardy, *Fundamentals of Two-Fluid Dynamics* (Springer-Verlag, Berlin, 1993).
[3] D. Johnson and R. Narayanan, "Marangoni convection in multiple bounded fluid layers and its application to materials processing," Philos. Trans. R. Soc. London, Ser. A **356**, 885 (1998).
[4] G. B. McFadden, S. R. Coriell, K. F. Gurski, and D. L. Cotrell, "Onset of convection in two liquid layers with phase change," Phys. Fluids **19**, 104109 (2007).
[5] G. B. McFadden, S. R. Coriell, and P. A. Lott, "Onset of convection in two layers of a binary liquid," J. Fluid Mech. **647**, 105 (2010).
[6] W. W. Mullins and R. F. Sekerka, "Stability of a planar interface during solidification of a dilute binary alloy," J. Appl. Phys. **35**, 444 (1964).
[7] F. Califano, R. Mauri, and R. Shinnar, "Large-scale, unidirectional convection during phase separation of a density-matched liquid mixture," Phys. Fluids **17**, 094109 (2005).
[8] J. S. Turner, *Buoyancy Effects in Fluids* (Cambridge University Press, Cambridge, England, 1973).
[9] L. D. Landau and E. M. Lifshitz, *Fluid Mechanics* (Butterworth-Heinemann, Oxford, 1987).
[10] C. Canuto, M. Y. Hussaini, A. Quarteroni, and T. A. Zang, *Spectral Methods. Fundamentals in Single Domains* (Springer-Verlag, Berlin, 2006).
[11] M. R. Scott and H. A. Watts, "Computational solution of linear two-point boundary-value problems via orthonormalization," SIAM (Soc. Ind. Appl. Math.) J. Numer. Anal. **14**, 40 (1977).
[12] S. R. Coriell and G. B. McFadden, "Morphological stability," in *Handbook of Crystal Growth 1. Fundamentals, Part B: Transport and Stability*, edited by D. T. J. Hurle (North-Holland, Amsterdam, 1994), pp. 785–857.
[13] G. B. McFadden, S. R. Coriell, K. F. Gurski, and D. L. Cotrell, "Convective instabilities in two liquid layers," J. Res. Natl. Inst. Stand. Technol. **112**, 271 (2007).
[14] W. A. Tiller, K. A. Jackson, J. W. Rutter, and B. Chalmers, "The redistribution of solute atoms during the solidification of metals," Acta Metall. **1**, 428 (1953).
[15] M. J. D. Powell, "A hybrid method for nonlinear equations," in *Numerical Methods for Nonlinear Algebraic Equations*, edited by P. Rabinowitz (Gordon and Breach, New York, 1970), pp. 87–114.